Title
The link between phenotype and fatty acid metabolism in advanced chronic kidney disease

Journal
Nephrology Dialysis Transplantation, 32(7)

ISSN
0931-0509

Authors
Chen, Dan-Qian
Chen, Hua
Chen, Lin
et al.

Publication Date
2017-07-01

DOI
10.1093/ndt/gfw415

Peer reviewed

Nephrol Dial Transplant (2017) 1–13
doi: 10.1093/ndt/gfw415

ndt
Nephrology Dialysis Transplantation

Original Article

The link between phenotype and fatty acid metabolism in advanced chronic kidney disease

Dan-Qian Chen[1,*], Hua Chen[1,*], Lin Chen[1], Nosratola D. Vaziri[2], Ming Wang[1], Xiang-Ri Li[3] and Ying-Yong Zhao[1]

[1]Key Laboratory of Resource Biology and Biotechnology in Western China, Ministry of Education, School of Life Sciences, Northwest University, Xi'an, Shaanxi, China, [2]Division of Nephrology and Hypertension, School of Medicine, University of California Irvine, Irvine, CA, USA and [3]School of Chinese Materia Medica, Beijing University of Chinese Medicine, Beijing, China

*These two authors contributed equally to this work.

Correspondence and offprint requests to: Ying-Yong Zhao; E-mail: zyy@nwu.edu.cn; zhaoyybr@163.com

ABSTRACT

Background. The kidney plays a central role in elimination of metabolic waste products and regulation of low-molecular weight metabolites via glomerular filtration, tubular secretion and reabsorption. Disruption of these processes results in profound changes in the biochemical milieu of the body fluids, which contribute to complications of chronic kidney disease (CKD) by inducing cytotoxicity and inflammation. Insight into the changes of the composition of metabolites and dysregulation of target genes and proteins enhances the understanding of the pathophysiology of CKD and its complications, and the development of novel therapeutic strategies. Chronic interstitial nephropathy is a common cause of CKD. The present study was designed to determine the effect of chronic interstitial nephropathy on the composition of serum metabolites and regulation of oxidative, inflammatory, fibrotic and cytoprotective pathways.

Methods. Male Sprague–Dawley rats were randomized to the CKD and control groups ($n = 8$/group). CKD was induced by administration of adenine (200 mg/kg body weight/day) by oral gavage for 3 weeks. The control group was treated with the vehicle alone. The animals were then observed for an additional 3 weeks, at which point they were sacrificed and kidney and serum samples were collected. Serum metabolomic and lipidomic analyses were performed using ultra-performance liquid chromatography-quadrupole time-of-flight high-definition mass spectrometry. Kidney tissues were processed for histological and molecular biochemical analyses.

Results. CKD rats exhibited increased plasma urea and creatinine concentrations, renal interstitial fibrosis, tubular damage and up-regulation of pro-inflammatory, pro-oxidant and pro-fibrotic pathways. Comparison of serum from CKD and control rats revealed significant differences in concentrations of amino acids and lipids including 33 metabolites and 35 lipid species. This was associated with marked abnormalities of fatty acid oxidation, and γ-linolenic acid and linoleic acid metabolism in CKD rats. Logistic regression analysis identified tetracosanoic acid, docosatrienoic acid, PC(18:3/14:1) and L-aspartic acid, tetracosanoic acid and docosatrienoic acid as novel biomarkers of chronic interstitial nephropathy.

Conclusions. Advanced CKD in rats with adenine-induced chronic interstitial nephropathy results in profound changes in the serum metabolome, activation of inflammatory, oxidative and fibrotic pathways, and suppression of cytoprotective and antioxidant pathways.

Keywords: chronic kidney disease, fatty acid oxidation, lipidomics, metabolomics, oxidative stress

INTRODUCTION

One of the main functions of the kidneys is elimination of the waste products derived from metabolism of endogenous and exogenous compounds. The kidneys modulate the level of circulating low-molecular weight metabolites by several mechanisms, including glomerular filtration, tubular secretion,

tubular reabsorption, catabolism and biosynthesis. Disruption of these processes in renal insufficiency results in significant changes in the concentration of numerous metabolites in the body fluids. In addition, the underlying cause and the nature of renal injury modify the composition of various metabolites. Chronic kidney disease (CKD) has emerged as a major public health problem worldwide. Early detection of renal disease, careful monitoring of renal function and response to therapeutic interventions are critical for timely diagnosis and prevention of progression and complications of CKD. Currently available markers of kidney function, i.e. serum creatinine and urea concentrations, are not adequately sensitive to detect early stages of kidney disease. Insight into the dynamic changes in regulation, interaction and function of target genes, proteins and metabolites can enhance the understanding of the pathophysiology of CKD and the development of novel therapeutic strategies [1].

Application of the 'omics'-based approaches, including genomics, transcriptomics, proteomics, metabolomics and lipidomics, has allowed global characterization of the complex biological systems and their changes in pathological processes at the molecular level. Complex networks comprising genomics and proteomics have previously been applied to study the functional basis of CKD at the molecular level [2, 3]. Unlike genes and proteins, metabolites serve as direct signatures of biochemical activity and are, therefore, easier to correlate with the corresponding phenotypes. Metabolomics and lipidomics have become powerful and promising analytic tools that have been widely used to investigate the mechanism and biochemical features of the disease processes.

Proton nuclear magnetic resonance spectroscopy and liquid chromatography–mass spectrometry (LC–MS)-based metabolomic techniques have been applied to characterize metabolic features of CKD [4, 5]. Among the various LC–MS platforms, ultra-performance liquid chromatography-quadrupole time-of-flight high-definition mass spectrometry (UPLC-QTOF/HDMS) is regarded as one of the best analytical tools in terms of selectivity, sensitivity and reproducibility [6–10]. Application of these tools has demonstrated perturbations in metabolism of phospholipids, fatty acids, amino acids and uremic toxins in CKD. CKD results in profound changes in lipid and lipoprotein metabolisms [11–15]. The associated lipid disorders, in turn, contribute to progression of CKD and its cardiovascular and other complications [16–18].

Chronic interstitial nephropathy is a relatively common cause of CKD in humans. Animals with adenine-induced nephropathy are commonly used as a model to study chronic interstitial nephropathy [19–21]. In the present study, CKD was induced in rats by administration of adenine. Blood biochemistry, kidney histopathology and western blot analysis were employed. UPLC-QTOF/HDMS-based plasma metabolomics and lipidomics were applied to investigate the metabolic profiles, identify differential metabolites and uncover the biochemical features of CKD in rats with chronic interstitial nephropathy. The differential and lipid-derived metabolites were identified to determine the connection between the key mediators of inflammation and oxidative stress and to illuminate the biochemical features of adenine-induced CKD.

MATERIALS AND METHODS

Animals and sample collection

Male Sprague–Dawley rats weighing 190–210 g were used in this study. They were fed standard laboratory chow diet *ad libitum* and housed in the vivarium with a 12-h light/dark cycle. They were randomized to the CKD and control groups ($n = 8$/group). The CKD rats were given 200 mg/kg body weight of adenine dissolved in 1% (w/v) gum acacia solution by oral gavage once a day for 3 weeks. The control group was treated with the vehicle alone. The animals were then observed for an additional 3 weeks at which point plasma samples were collected and stored at −80°C. Samples were used as the discovery phase for metabolomic and lipidomic studies. Plasma samples were also collected from an independent set of eight adenine-induced CKD rats and eight control rats, and the samples were used to validate differential metabolites identified in the discovery phase. All the experimental procedures were approved by the Ethical Committee of Northwest University and conducted according to the principles expressed in the Declaration of Helsinki.

Physiologic parameters

Body weight, urinary volume, kidney size and plasma biochemistry were analyzed as described in detail previously [22]. Inflammatory markers, tumor necrosis factor-alpha (TNF-α) and interleukin-6 (IL-6) were measured in the serum samples using commercially available ELISA kits according to the manufacturer's instructions.

Kidney histology and western blot analysis

Antibodies including nuclear factor (NF)-κB p65, Nrf2, transforming growth factor (TGF)-β1, etc. were purchased from Santa Cruz Biotechnology or Abcam Company. The cytoplasmic and nuclear extracts were prepared as follow. The tissues were homogenized on ice in tissue extraction reagent I (Invitrogen) containing 50 mM Tris–HCl (pH = 7.4), 250 mM NaCl, 5 mM $C_{10}H_{16}N_2O_8$, 2 mM Na_3VO_4, 1 mM NaF, 20 mM $Na_4P_2O_7$, 0.02% NaN_3, 1% NP-40, 0.1% $NaC_{12}H_{25}SO_4$, proprietary detergent and protease inhibitor cocktail (Sigma–Aldrich). Protein concentration of tissue homogenates was determined by DC protein assay kit (Bio-Rad), and 100 μg total protein was fractionated on 4–12% Novex Tris–Glycine gel at 120 V for 2 h and transferred to nitrocellulose membrane (Invitrogen). The membranes were incubated for 1 h in 1 × TBS, 0.05% Tween-20 and 5% non-fat milk blocking buffer and then overnight in the same buffer containing the primary antibodies against: IDOL (SAB4501317, Sigma–Aldrich), at 1:500 LDLR (Fitzgerald Inc.) at 1 μg/mL and β-actin (ab6276, Abcam) at 1:5000. The membrane was washed three times for 10 min in 1 × TBST before a 2-h incubation in 1 × TBST buffer containing horseradish peroxidase-conjugated antirabbit (1:3000) (ab6721, Abcam) and anti-mouse (1:2000) secondary antibodies. The membrane was washed three times, then visualized with ECLTM prime western blot detection reagent (RPN2232, GE Healthcare) and developed by autoluminography. Band densities were quantified using the free ImageJ

software (version 10.2). Hematoxylin–eosin staining (H&E), picro-sirius staining and immunohistochemistry were performed as described in detail previously [23].

Metabolomics analysis

Frozen plasma samples were allowed to thaw at 4°C overnight and then vortex mixed for 10 s before being sampled for the sample preparation procedure. The Ostro 96-well sample preparation plate is designed to capture and remove the highly abundant phospholipids as part of sample preparation for the analysis of small molecules during routine bioanalysis. Briefly, 100 µL plasma samples were added to a 2 mL Ostro Protein Precipitation 96-well plate (Waters Corporation). A 300 µL aliquot of methanol was added to all wells and mixed thoroughly with the sample by aspirating three times using an automated pipette and the plasma samples was repeatedly extracted three times. Samples were extracted using a vacuum manifold for approximately 5–7 min. The eluate from each collection plate insert was then transferred to glass LC-vials for UPLC analysis.

Each sample was injected onto a reverse-phase 100×2.1 mm, HSS 1.7 µm C_{18} column using an ACQUITY UPLC system (Waters Corporation). The gradient mobile phase comprised of water containing 0.1% formic acid solution (A) and acetonitrile (B). Each sample was resolved for 9 min at a flow rate of 0.45 mL/min. The mobile phase consisted of 0.1% formic acid water (A) and acetonitrile (B). The optimized UPLC elution conditions were: 0.0–7.0 min, 99.0–1.0% A; 7.0–8.0 min, 1.0% A and 8.0–9.0 min, 1.0–99.0% A. The autosampler was maintained at 4°C. Every 5 µL sample solution was injected for each run.

The column eluent was introduced directly into the mass spectrometer by electrospray. Mass spectrometry was performed on a Xevo^{TM} G2 QTOF/MS (Waters MS Technologies) operating in either negative or positive electrospray ionization mode with a capillary voltage of 3.0 kV and a sampling cone voltage of 35 V. The desolvation gas flow was 600 L/h and the temperature was set to 350°C. The cone gas flow was 50 L/h, and the source temperature was 100°C. The mass spectrometry was operated in W optics mode with 12 000 resolution using dynamic range extension. Data were acquired in continuum mode from 50 to 1000 m/z mass range for TOF-MS scanning, in duplicates (technical replicates) for each sample in positive and negative ionization mode and checked for chromatographic reproducibility. Leucine–enkephalin was used as the lockmass at a concentration of 300 ng/mL and flow rate of 5 µL/min. Data were collected in continuum mode, the lockspray frequency was set at 10 s, and data were averaged over 10 scans. All the acquisition and analysis of data were controlled by Waters Unifi software.

Lipidomics samples

Lipids extraction using Ostro 96-well plate was performed as a single-step in-well extraction. A total of 100 µL of plasma was loaded into each well of a 2 mL Ostro sample preparation plate fitted onto a vacuum manifold. A 300 µL of elution solvent (1:1, chloroform/methanol) of methanol was added to each well and mixed thoroughly by aspirating the mixture 10 times using a micropipette. A vacuum of approximately 15" Hg was applied to the plate until the solvent was completely drained. This step was repeated with another 300 µL of chloroform and methanol with the total fraction. This step was repeated three times and got the total fraction volume to ~900 µL. The eluate fraction was dried down under nitrogen, and reconstituted with 200 µL 1:1 (v/v) chloroform/methanol. This sample was then injected into the UPLC/MS system.

The UPLC analysis was performed in the above-mentioned chromatographic separation of metabolomic analysis. A gradient of 10 mM ammonium formate in 2-propanol/acetonitrile (90/10) in 0.1% formic acid (A) and 10 mM ammonium formate in ACN/H_2O (60/40) in 0.1% formic acid (B) was used as follows: a linear gradient of 0–10 min, 40.0–99.0% A and 10.0–12.0 min, 99.0–40.0% A. The flow rate was 0.5 mL/min. The temperatures of autosampler and chromatographic column were maintained at 4°C and 55°C, respectively. Every 5 µL sample solution was injected for each run.

For lipidomics analysis, mass spectrometry was performed on a Xevo^{TM} G2 QTof. The scan range was from 100 to 1500 m/z. For both positive and negative electrospray modes, the capillary and cone voltage were set at 3.0 kV and 60 V, respectively. The desolvation gas was set to 900 L/h at a temperature of 500°C; the cone gas was set to 50 L/h and the source temperature was set to 120°C. An MS^E experiment was performed as follows: function 1, 10 V collision energy; function 2, collision energy ramp of 20–65 V. Data were collected in continuum mode, the lockspray frequency was set at 10 s, and data were averaged over 10 scans. All the acquisition and analysis of data were controlled by Waters Unifi software.

Data analysis

The acquired UPLC-QTOF/HDMS positive electrospray ionization (ESI+) mode and negative electrospray ionization (ESI-) mode raw data were first pre-processed by the Progenesis QI and Markerlynx XS (Waters Corporation) as described in a previous publication [22]. Orthogonal partial least squares-discriminant analysis (OPLS-DA) was performed to discriminate between CKD group and control group. The potential differential metabolites between groups were identified on the basis of variable importance in the projection (VIP) values from the 7-fold cross-validated OPLS-DA model on the normalized peak intensity, where metabolites with VIP > 1.0 were selected. A panel of potential metabolites responsible for the difference in the CKD group and control group was obtained.

Fold change was calculated as a binary logarithm of the average normalized peak intensity ratio between CKD group and control group. Based on the normalized peak intensity, One-way analysis of variance (ANOVA) in the SPSS software (version 19.0, IBM) was also applied to calculate the statistical significance of each metabolite. The resultant P-values from ANOVA were further adjusted using the Hochberg and Benjamini false discovery rate method. Potential metabolites with both multivariate and univariate statistical significance (VIP > 1 and $P < 0.05$) were considered to be potential biomarkers in the adenine-induced CKD. Class-specific metabonomic and lipidomic patterns were visualized using heat map with Metaboanalyst software (version 3.0) and *z*-score plots with R software (version 2.15.0). In addition, receiver operator

characteristic (ROC) analysis was performed for the selection of candidate biomarkers, and ROC curves were plotted using a nonparametric method by using the SPSS software (version 19.0, IBM). In addition, correlation analyses were investigated by using the peak area of metabolites and the concentration of clinical biochemistry including renal function parameter creatinine and lipid metabolism parameter triglyceride and total cholesterol.

The related metabolic pathways in rats with adenine-induced CKD were performed by means of the quantitative enrichment analysis (QEA) algorithm described in the metabolite set enrichment analysis (MSEA) method [24]. Visualization of the remarkably disturbed metabolic pathways in rats with adenine-induced CKD was performed by MetScape software (version 3.1) running on cytoscape [25].

RESULTS

General data

Body weight was significantly reduced and urinary volume was significantly increased in CKD rats compared with the controls. Similarly, compared with the control rats, the weight, length and width of the kidneys were markedly increased in CKD rats (Table 1). Compared with the control rats, serum concentrations of urea, creatinine, uric acid, triglyceride, cholesterol, potassium and phosphorus were markedly increased, whereas creatinine clearance and serum calcium were significantly reduced in CKD rats (Table 1). No significant difference was found in serum sodium and chloride concentrations between the CKD and control rats. Significantly increased white blood cell count and decreased red blood cell count were found in CKD rats (Table 1). The serum TNF-α and IL-6 levels were significantly higher in CKD rats compared with controls rats. These findings reflect the CKD-associated anemia and systemic inflammation.

Histological findings

Figure 1 shows representative H&E-, periodic acid–Schiff (PAS)-, Masson- and immunohistochemistry-stained sections of the kidneys from control and CKD rats. CKD rats showed severe tubular atrophy and dilation, epithelial denudation, interstitial fibrosis, inflammatory cell infiltration and granuloma formation. PAS staining showed extensive peri-arteriolar and tubulointerstitial fibrosis in CKD rats. Masson staining showed severe tubulointerstitial fibrosis in CKD rats. This was associated with a significant increase in the numbers of macrophages (ED-1-positive cells) (Figure 1).

Expression of pro-inflammatory, pro-oxidant and fibrotic proteins

The kidney tissues in CKD rat showed a significant increase in nuclear translocation of p65, indicating activation of NF-κB. Activation of NF-κB was accompanied by significant up-regulation of inflammatory proteins including monocyte chemotactic protein-1 (MCP-1), inducible nitric oxide synthase (iNOS), cyclooxygenase-1 (COX-1) and cyclooxygenase-2 (COX-2), up-regulation of pro-oxidant proteins including NADPH oxidase 4 (NOX4), gp91^{Phox} and P47^{Phox}, and down-regulation of the anti-oxidant system including Nrf2, glutathione peroxidase (GPX), catalase, Cu/Zn SOD and heme oxygenase-1 (HO-1), and accumulation of nitrotyrosine (Figure 2A and B). Activation of inflammatory and oxidative pathways in CKD rats was accompanied by significant up-regulation of ED-1, and TGF-β1, plasminogen activator inhibitor-1 (PAI-1) and α-smooth muscle actin (α-SMA) (Figures 1 and 2C). Taken together, these findings point to activation of the pro-inflammatory, pro-oxidant and fibrotic pathways and down-regulation of Nrf2-mediated antioxidant and phase 2 detoxifying enzymes and related proteins.

Table 1. Body weight, urinary volume, kidney size, plasma biochemistry, erythrocyte count and leukocyte count in the control (CTL) and CKD groups

Parameter	CTL group	CKD group
Body weight (g)	347±21	235±29**
Urinary volume (mL)	15.5±4.2	46.2±10.8**
Kidney weight index (g/g × 100)	0.83±0.05	4.34±0.52**
Kidney length index (mm/g × 100)	5.3±0.3	9.9±0.8**
Kidney width index (mm/g × 100)	2.9±0.2	6.3±0.5**
Serum urea (mmol/L)	6.4±1.8	37.5±5.2**
serum creatinine (μmol/L)	33.2±2.4	125.6±14.3**
Creatinine clearance rate (mL/min/kg)	2.54±0.29	1.52±0.18**
Serum triglyceride (mmol/L)	0.41±0.08	1.12±0.19**
Serum cholesterol (mmol/L)	1.98±0.39	2.52±0.43*
Serum uric acid (μmol/L)	124.5±15.5	179.6±19.9**
Serum potassium (mmol/L)	5.14±0.23	5.94±0.41**
Serum sodium (mmol/L)	139±2	142±2
Serum chloride (mmol/L)	101±1	103±2
Serum phosphorus (mmol/L)	1.93±0.43	3.25±0.73**
Serum calcium (mmol/L)	2.43±0.05	2.29±0.07*
Serum creatine kinase (mmol/L)	1965±235	2296±268*
White blood cell (10^9/L)	12.7±2.2	22.3±3.3**
Red blood cell (10^{12}/L)	7.8±0.3	6.4±0.4**
Serum IL-6 (pg/mL)	8.54±1.25	18.68±3.76**
Serum TNF-γ (pg/mL)	7.62±1.46	25.87±6.56**
Urine creatinine (μmol/L)	3267.8±748.9	1201.1±189.8**
Urine urea (mmol/L)	244.4±27.3	209.7±25.1

Results are expressed as the means ± standard deviation.
*$P < 0.05$, **$P < 0.01$ compared with control rats by unpaired Student's *t*-test. Kidney weight index = kidney weight (g)/body weight (g) × 100; kidney length index = kidney length (mm)/body weight (g) × 100; kidney width index = kidney length (mm)/body weight (g) × 100.

Multivariate analysis and biomarker identification for metabolomics and lipidomics

OPLS-DA was employed for the analysis of metabolic profiles and identification of metabolite changes. Using the VIP values (VIP > 1) derived from the S-plot and the P-values ($P < 0.05$), 39 differential metabolites were identified in CKD rats (Supplementary Table S1). The heatmap presents the relative intensity of identified metabolites showing the relative increase (red) or decrease (green) in CKD rats compared with the control rats (Figure 3A). Thirty-four lipid metabolites were identified that belong to the five lipid classes: 19 glycerophospholipids, 5 sphingolipids, 5 fatty acids, 3 sterol lipids and 2 glycerolipids. Metabolomics revealed that 34 of the identified metabolites that were altered in CKD rats were lipids,

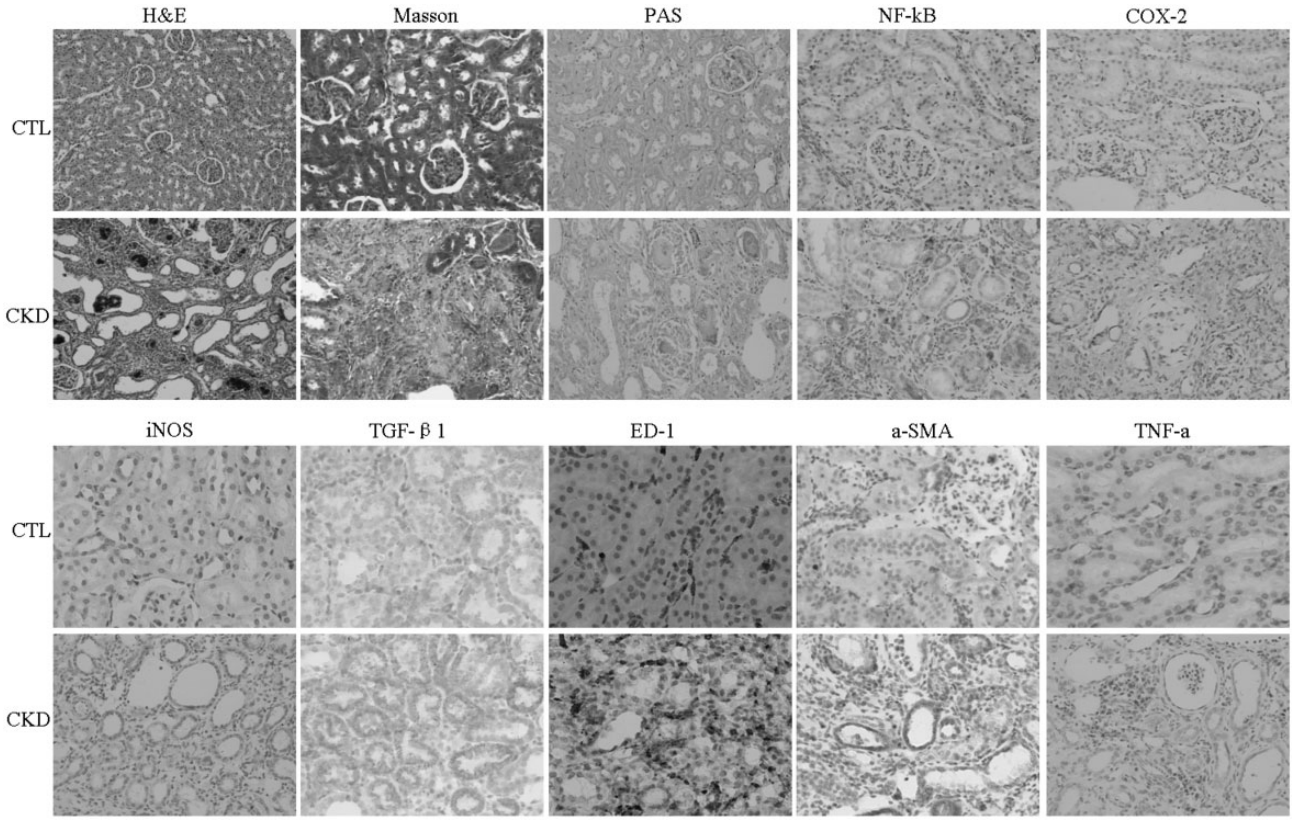

FIGURE 1: Representative photomicrographs of the kidney sections from control (CTL) and CKD rats stained with H&E, PAS and Masson staining as well as NF-KB, COX-2, iNOS, TGF-β1, ED-1, α-SMA and TNF-α immunohistochemistry. The kidney in the tubulointerstitial nephropathy rats showed significant tubulointerstitial injury by heavy inflammatory cell infiltration, tubular dilation and fibrosis.

accounting for 87.2% of all identified metabolites affected by CKD. Figure 3C represents the *z*-score plots of the altered metabolites in CKD compared with the control group. The plots display the relative intensities of the identified metabolites that were different between CKD and control rats. Figure 3E shows the mean ratio of each analyte in CKD versus control rats, plotted against their minus logarithm of P-value (Supplementary Table S1). Thirty-four metabolites achieved a conservative Bonferroni-adjusted significance threshold of $P < 0.000128$ (0.05/39 metabolites), with 33 of these metabolites higher in CKD rats compared with control rats (Table 2). The results indicated that the metaolic profile was significantly disturbed in rats with chronic interstitial nephropathy. Therefore, lipid metabolism was further studied using lipidomics approach. Using the VIP values and the P-values ($P < 0.05$), 40 differential lipid metabolites from ESI^+ mode and 19 differential lipid metabolites from ESI^- mode were identified (Supplementary Table S2). The heatmap presents 59 differential lipids showing the relative increase (red) or decrease (green) in CKD rats compared with control rats (Figure 3B). The heatmap allowed better differentiation of the lipid profile between the CKD and control rats. Fifty-nine differential lipid metabolites belong to the six lipid classes: 26 glycerolipids, 22 glycerophospholipids, 2 sterol lipids, 2 fatty acids, 1 prenol lipid and 1 eicosanoid. The difference in plasma concentrations of these 59 lipid species between CKD and control rats was highly significant. The change in plasma concentration (increase or decrease) of the lipids between CKD and control rats was more than 1.4 times (Figure 3D). Figure 3F shows the mean ratio of each analyte in CKD rats versus control rats, plotted against their minus logarithm of P-value (Supplementary Table S2). Thirty-five metabolites achieved a conservative Bonferroni-adjusted significance threshold of $P < 0.000847$ (0.05/59 metabolites), with 34 of these metabolites being higher in CKD compared with control rats (Table 3). The results indicated that the lipid profile was significantly disturbed in rats with chronic interstitial nephropathy.

Validation of significantly altered metabolites

To test the usefulness of these differential metabolites, an additional eight adenine-induced CKD rats and eight control rats were used for validating these significantly altered metabolites. Principal component analysis (PCA) score plots indicated that 33 differential metabolites (Figure 4A) and 35 differential lipid species (Figure 4B) could separate CKD rats from control rats. Predicted class probabilities were performed on 33 differential metabolites (Figure 4C) and 35 differential lipid species (Figure 4D) from eight independent adenine-induced CKD rats and eight control rats. All eight CKD samples were correctly grouped (100% sensitivity). All eight control samples were located in the control area (100% specificity). The suitability of the differential metabolites was further validated by ROC analysis. The metabolomic ROC results showed that differential metabolites were robust in distinguishing CKD from control groups, with area under the curve (AUC), sensitivity and specificity values of 0.885 [95% confidence interval (CI):

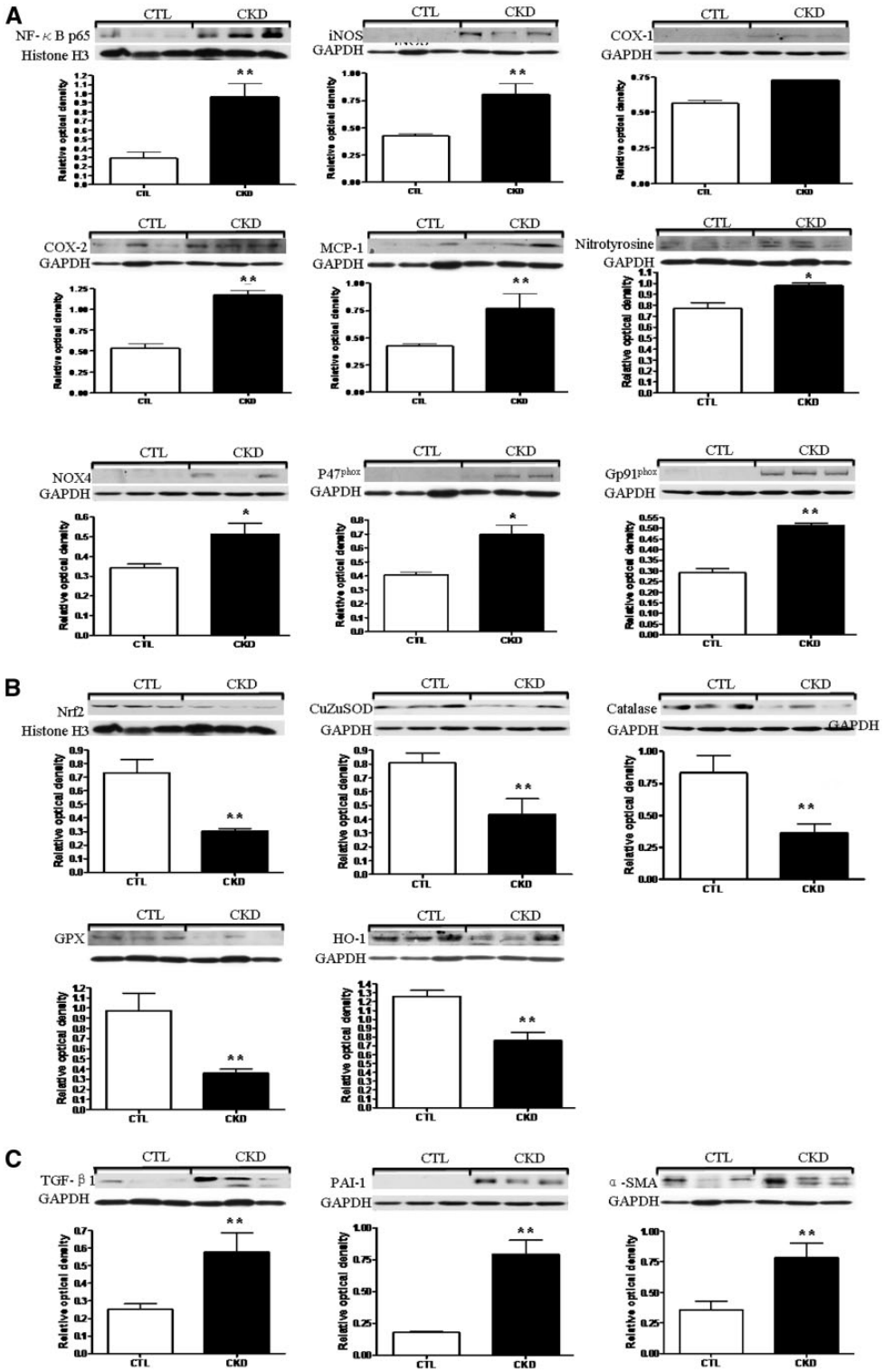

FIGURE 2: Expression of pro-inflammatory, pro-oxidant and fibrotic proteins in kidney tissues. Representative western blots of pro-inflammatory and pro-oxidant proteins including NF-κB, iNOS, COX-1, COX-2, MCP-1, NOX4, gp91^{Phox}, P47^{Phox} and nitrotyrosine (**A**), anti-oxidative stress proteins including Nrf2, GPX, catalase, Cu/Zn SOD and HO-1(**B**) and pro-fibrotic proteins including TGF-β1, PAI-1 and α-SMA (**C**) in control (CTL) and CKD groups ($n = 8$). Histone H3 and GAPDH served as the loading control. *$P < 0.05$, **$P < 0.01$.

0.829–0.892], 93.3%, and 85.5%, respectively (Figure 4E). Similarly, differential lipid species exhibited high diagnostic performance in distinguishing CKD from control groups, with AUC, sensitivity and specificity values of 0.913 (95% CI: 0.848–0.934), 99.9% and 93.8%, respectively (Figure 4F).

Selection of biomarker candidates by logistic regression model

To assess the potential utility of altered metabolites as predictive markers of CKD, we produced a logistic regression model based on the 33 validated metabolites or 35 lipid species from

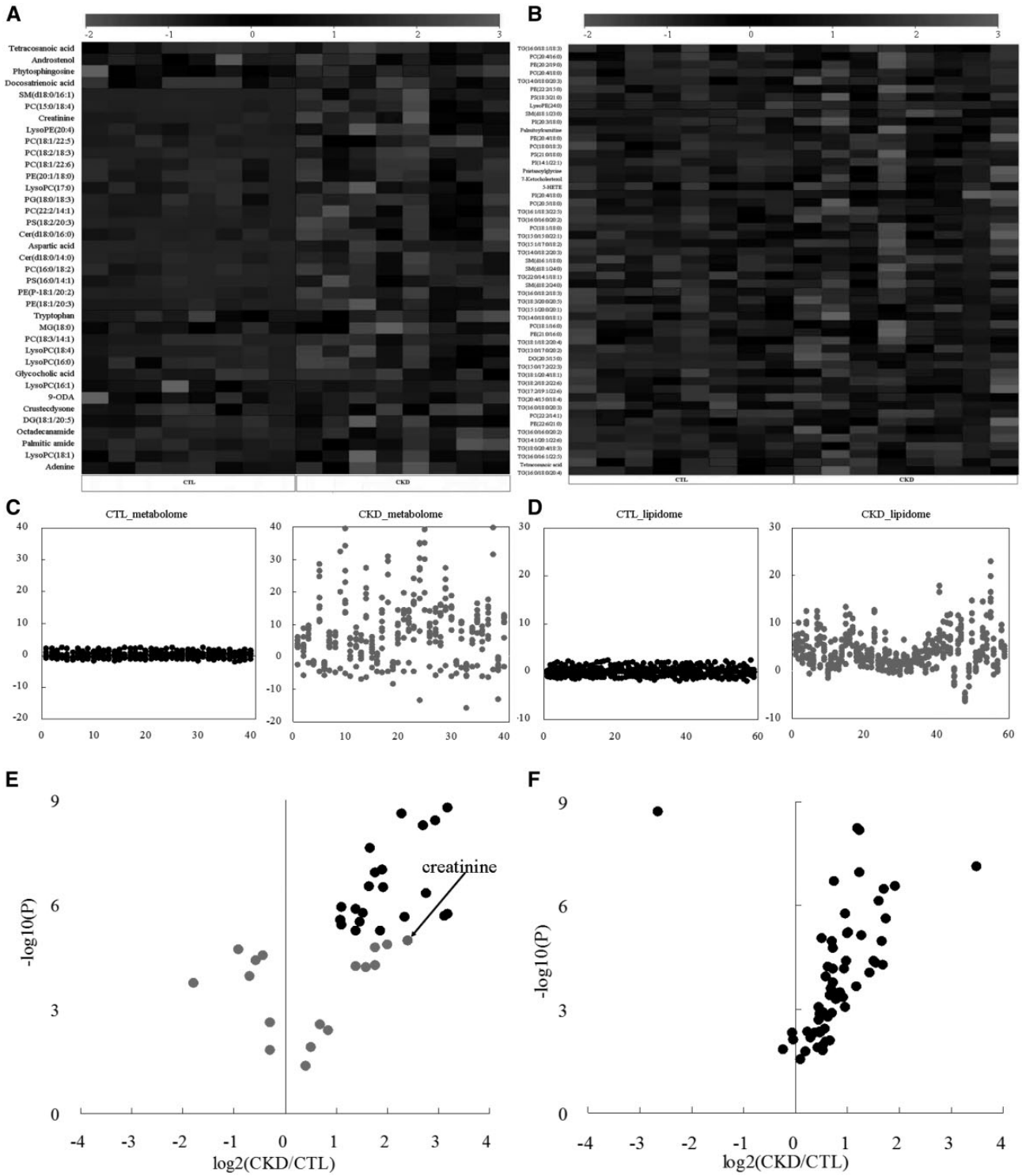

FIGURE 3: Multivariate analysis and significantly altered metabolite identification. The heatmap represented hierarchical clustering of the differential metabolites from metabolomics (**A**) and lipidomics (**B**) in control (CTL) and CKD groups. Each line of this graphic represents a relationship of different metabolites, colored by their relative intensities (red, upregulated; green, downregulated). Columns: plasma samples; rows: metabolites. 9-ODA, 9-oxooctadecanoic acid. *Z*-score plots of metabolomic and lipidomic alterations in CKD rats. Each point represents one metabolite or one lipid in one CTL or CKD sample. (**C** and **D**) *Z*-score plots for the data normalized to the mean of the CTL samples. *x*-Axis, metabolites; *y*-axis, relative intensities. The geometric mean ratio of each metabolite in CKD versus CTL was presented in metabolomics (E) and lipidomics (**F**). The *y*-axis shows minus logarithm of P-value. The *x*-axis shows the logarithm of ratio of CKD/CTL of each plasma sample. The $\log_2$(CKD/CTL) with a value >0 indicated a relatively higher intensity present in CKD rats, whereas a value <0 indicated a relatively lower intensity compared with the control rats.

Table 2. Differential plasma metabolites of rats with adenine-induced CKD detected by UPLC-MS in positive ionization mode

Compounds	VIP[a]	Ratio (CKD/CTL)	P[b]
Tetracosanoic acid	3.34	2.62	1.35E-06
Palmitic amide	1.62	2.61	5.94E-06
Octadecanamide	1.55	3.19	2.47E-08
Docosatrienoic acid	3.17	0.53	2.07E-05
9-Oxooctadecanoic acid	1.5	0.62	1.14E-04
PC(22:2/14:1)	1.77	4.04	1.49E-05
PC(18:3/14:1)	3.35	4.88	2.53E-09
PC(18:2/18:3)	1.32	9.05	1.66E-09
PC(18:1/22:6)	1.49	3.39	1.27E-07
PC(18:1/22:5)	1.45	2.75	3.29E-06
PC(16:0/18:2)	1.79	6.50	5.27E-09
PC(15:0/18:4)	2.78	6.76	5.04E-07
LysoPE(20:4)	1.97	3.02	6.63E-05
LysoPC(18:4)	3.17	5.08	2.33E-06
LysoPC(17:0)	1.66	3.63	5.64E-06
LysoPC(16:1)	3.31	0.29	1.82E-04
LysoPC(16:0)	2.96	2.16	3.89E-06
PE(P-18:1/20:2)	1.73	2.88	1.82E-06
PE(20:1/18:0)	1.47	3.12	3.08E-07
PE(18:1/20:3)	2.25	3.42	1.72E-05
PS(18:2/20:3)	1.91	8.73	2.15E-06
PS(16:0/14:1)	1.82	3.79	3.22E-07
PG(18:0/18:3)	1.45	2.12	2.87E-06
Cer(d18:0/16:0)	1.59	3.40	5.87E-05
Cer(d18:0/14:0)	1.57	7.71	4.05E-09
SM(d18:0/16:1)	1.88	3.72	1.05E-07
DG(18:1/20:5)	2.37	2.62	6.02E-05
Dihydrosphingosine	1.69	9.04	1.87E-06
Androstenol	1.90	0.67	4.11E-05
Crustecdysone	1.48	0.74	2.92E-05
Glycocholic acid	2.83	2.16	1.23E-06
L-Aspartic acid	1.46	5.92	7.29E-11
Creatinine	2.56	5.26	1.10E-05

[a]VIP value was obtained from OPLS-DA model.
[b]P-values are calculated from a one-way ANOVA.
[c]The false discovery rate (FDR) value was obtained from the adjusted P-value of FDR correction using Benjamini Hochberg method.
CTL, control.

Table 3. Differential lipids of rats with of adenine-induced CKD detected by UPLC-MS in positive ionization mode and negative ionization modes

Compounds	VIP[a]	Ratio (CKD/CTL)	P[b]
TG(22:0/14:1/18:1)	2.03	1.50	1.15E-04
TG(18:2/18:2/22:6)	1.06	1.73	5.37E-04
TG(18:1/20:4/18:1)	1.99	1.65	1.75E-04
TG(18:0/20:4/18:3)	2.84	2.34	1.14E-07
TG(17:2/19:1/22:6)	1.78	1.58	3.98E-04
TG(16:0/16:1/22:5)	2.69	2.02	6.26E-06
TG(16:0/16:0/20:2)	2.93	1.91	7.09E-05
TG(16:0/16:0/20:2)	1.65	1.63	1.10E-05
TG(15:0/17:2/22:3)	2.22	2.29	6.00E-09
TG(14:1/20:1/22:6)	2.79	1.81	3.31E-04
TG(14:0/18:2/20:3)	1.99	3.28	3.49E-07
TG(13:0/17:0/20:2)	2.19	1.43	8.86E-06
DG(20:5/15:0)	2.63	2.71	8.89E-05
PC(22:5/20:5)	1.11	3.03	7.67E-07
PC(20:5/18:0)	1.25	1.91	4.60E-04
PC(20:4/18:0)	3.19	1.68	2.00E-07
PC(18:1/18:0)	2.28	2.42	7.52E-06
PC(18:1/16:0)	2.79	1.96	3.99E-05
PC(18:0/18:3)	1.69	1.95	1.81E-06
PE(22:2/15:0)	2.96	1.66	7.03E-05
PE(22:0/22:1)	1.47	11.2	7.69E-08
PE(20:4/18:0)	1.54	2.27	2.33E-04
PE(20:2/19:0)	2.98	2.00	6.44E-06
LysoPE(24:0)	1.8	0.16	1.91E-09
SM(d18:1/24:0)	1.48	1.62	2.57E-04
SM(d18:1/23:0)	1.75	3.34	2.41E-06
SM(d16:1/18:0)	1.55	1.65	1.74E-05
PS(21:0/18:0)	1.95	3.19	1.13E-05
PS(20:3/22:6)	1.16	3.79	2.78E-07
PS(18:3/21:0)	3.00	1.55	6.29E-05
PI(20:4/18:0)	3.67	1.63	2.99E-04
PI(14:1/22:1)	1.82	2.35	6.55E-09
Palmitoylcarnitine	1.69	3.22	5.30E-05
Pristanoylglycine	2.69	2.94	4.75E-05
7-Ketocholesterol	2.83	2.85	4.04E-05

[a]VIP value was obtained from OPLS-DA model.
[b]P-values are calculated from a one-way ANOVA.
CTL, control.

discovery phase and validation phase in CKD and control rats. Based on the forward stepwise analysis, tetracosanoic acid, L-aspartic acid, creatinine, PC(18:3/14:1) and docosatrienoic acid were identified as the best predictors of CKD in the regression model. In addition to the current standard biomarker, creatinine, two fatty acids (tetracosanoic acid and docosatrienoic acid), one glycerophosphocholine PC(18:3/14:1) and one amino acid L-aspartic acid were found as the biomarker candidates of CKD.

Correlation analyses between biomarker candidates and standard biochemical parameters

To further understand the relationship between four metabolites and the well-known biochemical abnormalities, we explored the correlation between the peak level of these metabolites and the concentration of creatinine, triglyceride and total cholesterol (Figure 5). Except for PC(18:3/14:1), tetracosanoic acid, docosatrienoic acid and L-aspartic acid were positively or negatively correlated with creatinine concentration ($R > 0.9498$). Except for L-aspartic acid, tetracosanoic acid, docosatrienoic acid and PC(18:3/14:1) were positively or negatively correlated with triglyceride concentration ($R > 0.9441$). Two fatty acids, tetracosanoic acid and docosatrienoic acid, showed good correlation with total cholesterol concentration ($R > 0.9449$). These results demonstrated strong correlation between these four metabolites with creatinine, triglyceride and total cholesterol.

Metabolic pathway analysis

To understand the functional impact of the alterations of the above plasma metabolites, the KEGG metabolic library was used by Metaboanalyst. We evaluated both a test for significantly altered metabolites in a pathway based on the hypergeometric tests and for the impact of the altered metabolites on the pathway function via alterations in important junction points of the pathway. Each of the 81 rat metabolic pathways in KEGG was simultaneously plotted to indicate the most significant pathways based on P-values of hypergeometric test (*y*-axis, red shades) and impact (*x*-axis, circle diameter) (Figure 6A). The top six pathways in plasma identified by P-value (top five) or impact (top one) include the following: (i) glycerophospholipid metabolism; (ii, iii) unsaturated fatty acids biosynthesis (linoleic acid and γ-linolenic acid metabolism); (iv) GPI-anchor

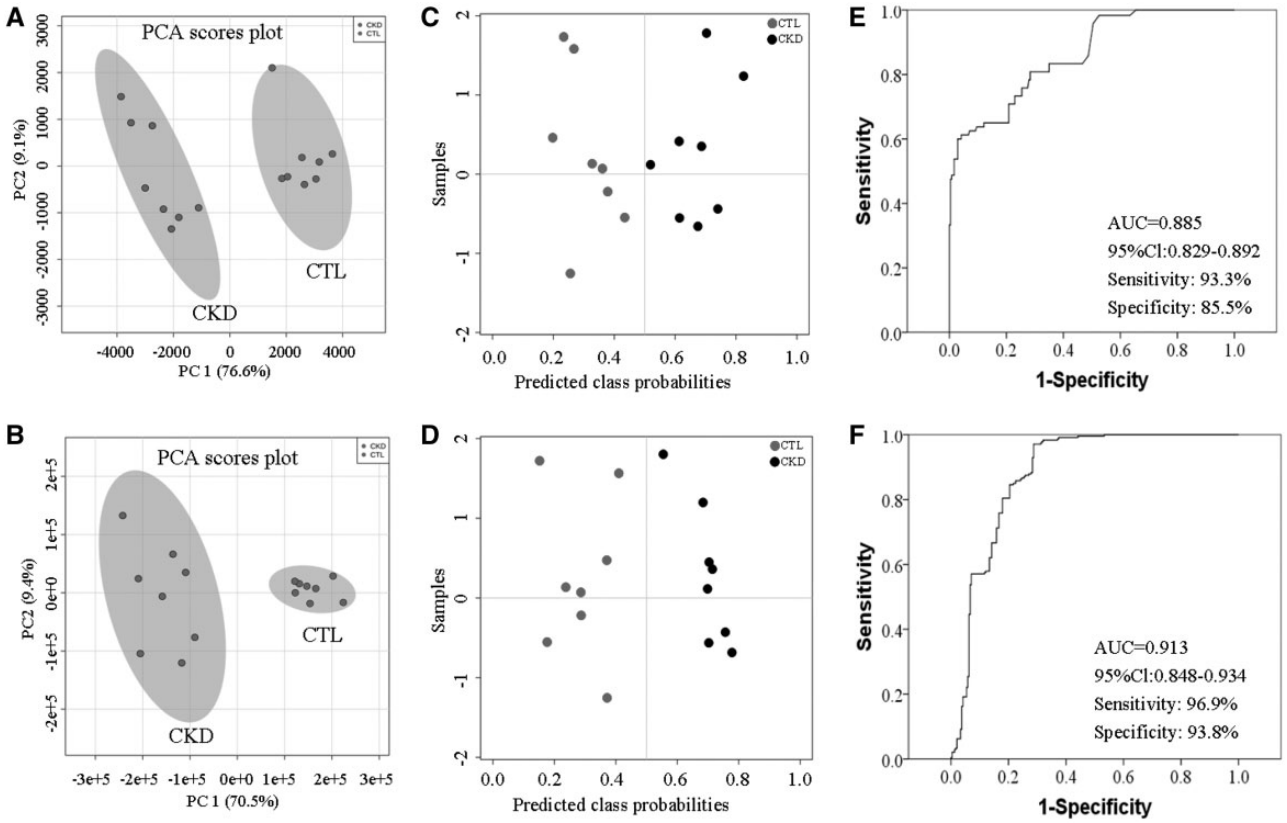

FIGURE 4: Differential metabolites were validated using an independent group. The PCA score scatter plot using 33 differential metabolites (**A**) and 35 differential lipid metabolites (**B**) from plasma sample between the CKD rats and control (CTL) rats. PCA score plots indicated that altered metabolites could separate CKD rats from CTL rats. Validation of diagnostic performances of the 33 differential metabolites (**C**) and 35 differential lipid metabolites (**D**) based on the partial least squares-discriminant analysis (PLS-DA) model. Validation of ROC curve analysis of the 33 differential metabolites (**E**) and 35 differential lipid metabolites (**F**) for the predictive power of potential biomarkers in CKD. Thirty-three differential metabolites obtained an AUC value of 0.885 (95% CI: 0.829 – 0.892) with 93.3% sensitivity and 85.5% in distinguishing CKD from CTL. Thirty-five differential lipid metabolites obtained an AUC value of 0.913 (95% CI: 0.848 – 0.934) with 99.9% sensitivity and 93.8% in distinguishing CKD from CTL.

biosynthesis; (v) histidine metabolism; and (vi) β-alanine metabolism. These altered plasma pathways in CKD rats indicate that disturbance of certain central metabolites produces an important impact on multiple metabolic pathways that are interconnected. Most of the altered metabolites were fatty acids and amino acids, indicating that fatty acid and amino acid metabolisms were heavily perturbed in CKD rats. A pathway enrichment overview of the altered metabolites revealed marked alterations of malate-aspartate metabolism and long-chain fatty acids β-oxidation in CKD rats (Figure 6B). In addition, metabolic pathways of the differential metabolites were visualized by using Cytoscape software. Part of metabolic pathways including disorders of amino acid, adenine and lipid metabolisms are shown in Figure 6C. The main pathway of lipid metabolism affected by CKD included glycerophospholipid metabolism and unsaturated fatty acids biosynthesis (linoleic acid and γ-linolenic acid metabolism).

DISCUSSION

Inflammation plays an important role in the progression of CKD and many of its adverse complications. The current western blot and metabolomics data demonstrated the presence of inflammation in the kidney tissues of CKD rats. The kidney tissues of our CKD rats with chronic interstitial nephropathy showed a significant increase in nuclear translocation of p65 (NF-κB activation), up-regulation of inflammatory, pro-oxidant and pro-fibrotic proteins, and down-regulation of anti-oxidant system. Oxidative stress and inflammation are common features and the major mediators of morbidity and mortality in CKD patients [26]. Oxidative stress is caused by an imbalance between oxidant production and antioxidant defence system [27]. Oxidative stress in CKD is due to a combination of excess production of reactive oxygen species (ROS) and deficient anti-oxidant defence system, which is caused by impaired Nrf2 activity [28, 29]. Several studies have demonstrated oxidative stress in patients with CKD [30, 31], as evidenced by accumulations of reactive carbonyl compounds, thiobarbituric acid-reactive substances and malondialdehyde in plasma, pointing to increased protein and lipid peroxidation.

Oxidative stress and inflammation in our CKD group was associated with marked alteration of plasma concentrations of different metabolites. Tetracosanoic acid, L-aspartic acid, creatinine, PC(18:3/14:1) and docosatrienoic acid were identified by logistic regression model as the biomarker candidates for CKD.

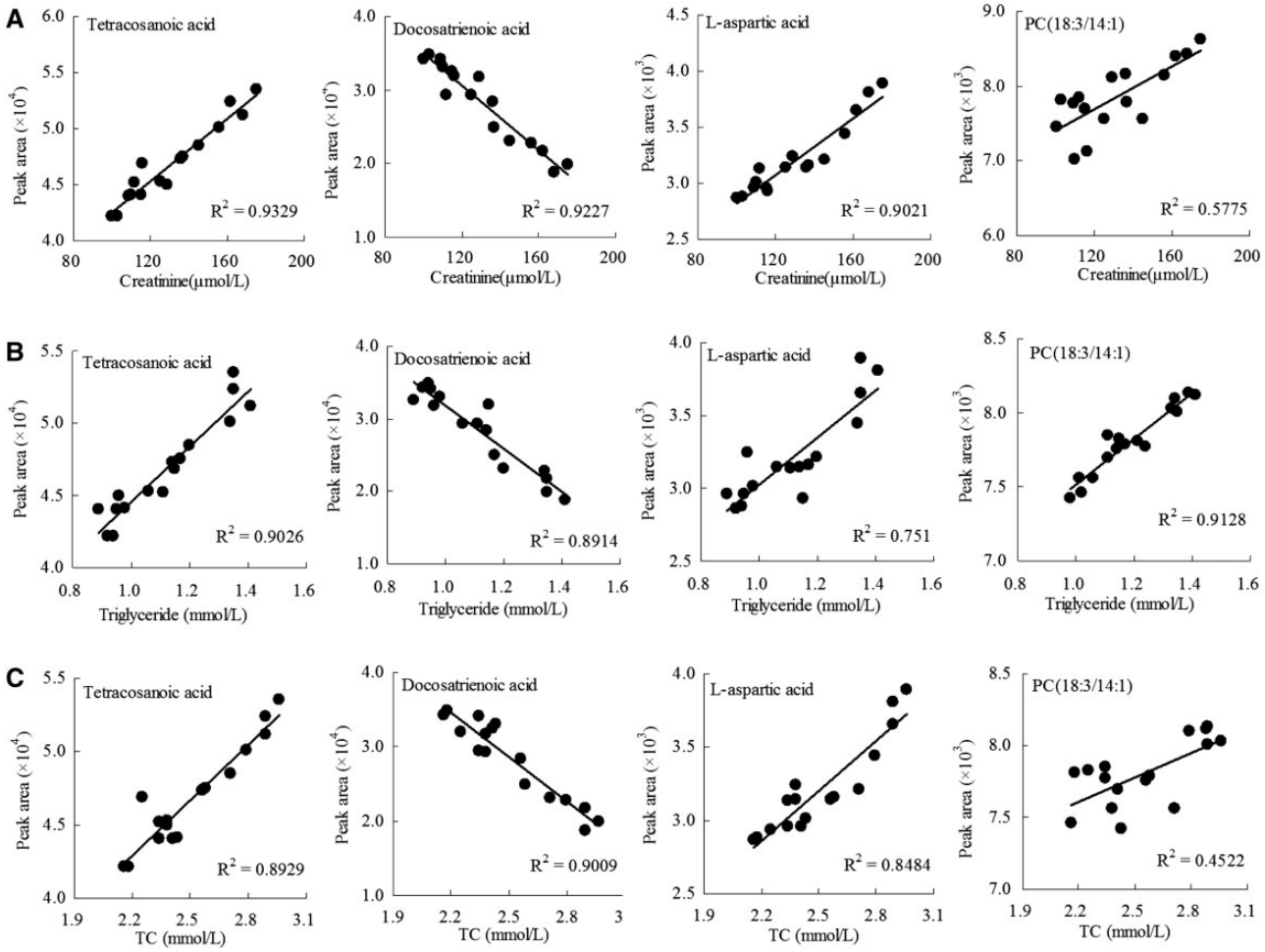

FIGURE 5: Significantly altered metabolites were well correlated with clinical biochemistry. Correlation between tetracosanoic acid, docosatrienoic acid, PC(18:3/14:1) and L-aspartic acid levels (peak area) measured by the UPLC-HDMS and serum creatinine (**A**), triglyceride (**B**) and total cholesterol (TC) (**C**) measured by clinical laboratory from the 16 CKD rats of discovery phase and validation phase. The correlation coefficient is shown in each graph.

Further correlation analysis showed strong association of the four metabolites with creatinine, triglyceride and total cholesterol concentrations. Therefore, they could be considered as additional biomarkers of advanced CKD.

Based on the multiple step metabolite selection and cross validation model, among lipid species, fatty acids were significantly altered by CKD. Our study showed that plasma levels of saturated fatty acids including tetracosanoic acid, octadecanamide, palmitic amide and palmitoylcarnitine were significantly increased, whereas polyunsaturated fatty acids (PUFA), including docosatrienoic acid level, were significantly decreased in CKD rats. This is consistent with earlier studies that have shown marked elevation of plasma free fatty acids and saturated fatty acids in the pre-hemodialysis blood samples from end-stage renal disease patients compared with controls [32]. In fact, blood level of saturated fatty acids has been shown to be associated with the odds of sudden cardiac death in patients maintained on hemodialysis [33].

Based on Kyoto Encyclopedia of Genes and Genomes (KEGG) metabolic and enrichment pathway analyses, we found marked changes in fatty acid oxidation and γ-linolenic acid and linoleic acid (ω-3 and ω-6) metabolism in CKD rats, indicating that this pathway could be considered as a therapeutic target for CKD. Recently, Kang *et al.* [34] showed reduced expression of key enzymes and regulators of fatty acid oxidation and increased intracellular lipid deposition in both humans and mice with tubulointerstitial fibrosis. Moreover, using *in vitro* experiments they found that inhibition of fatty acid oxidation in cultured renal tubular epithelial cells caused ATP depletion, cell death, dedifferentiation and intracellular lipid deposition, phenotypes observed in fibrosis. In contrast, restoration of fatty acid metabolism by genetic or pharmacological methods protected mice from tubulointerstitial fibrosis [34]. Long-chain fatty acid uptake is facilitated by the long-chain fatty acid transporter CD36 [35]. Fatty acid metabolism requires their transport into the mitochondria by linking fatty acids to carnitine via carnitine palmitoyltransferase-1, which is the rate-limiting enzyme in fatty acid oxidation [36]. Diabetes results in mitochondrial dysfunction, which leads to impaired β-oxidation of fatty acids and oxidative phosphorylation defect, events that contribute to the development of kidney disease [37]. Plants and fish are two major sources of ω-3 fatty acids γ-linolenic acid and eicosapentaenoic acid and docosahexaenoic acid, respectively. In mammals, γ-linolenic acid is converted through

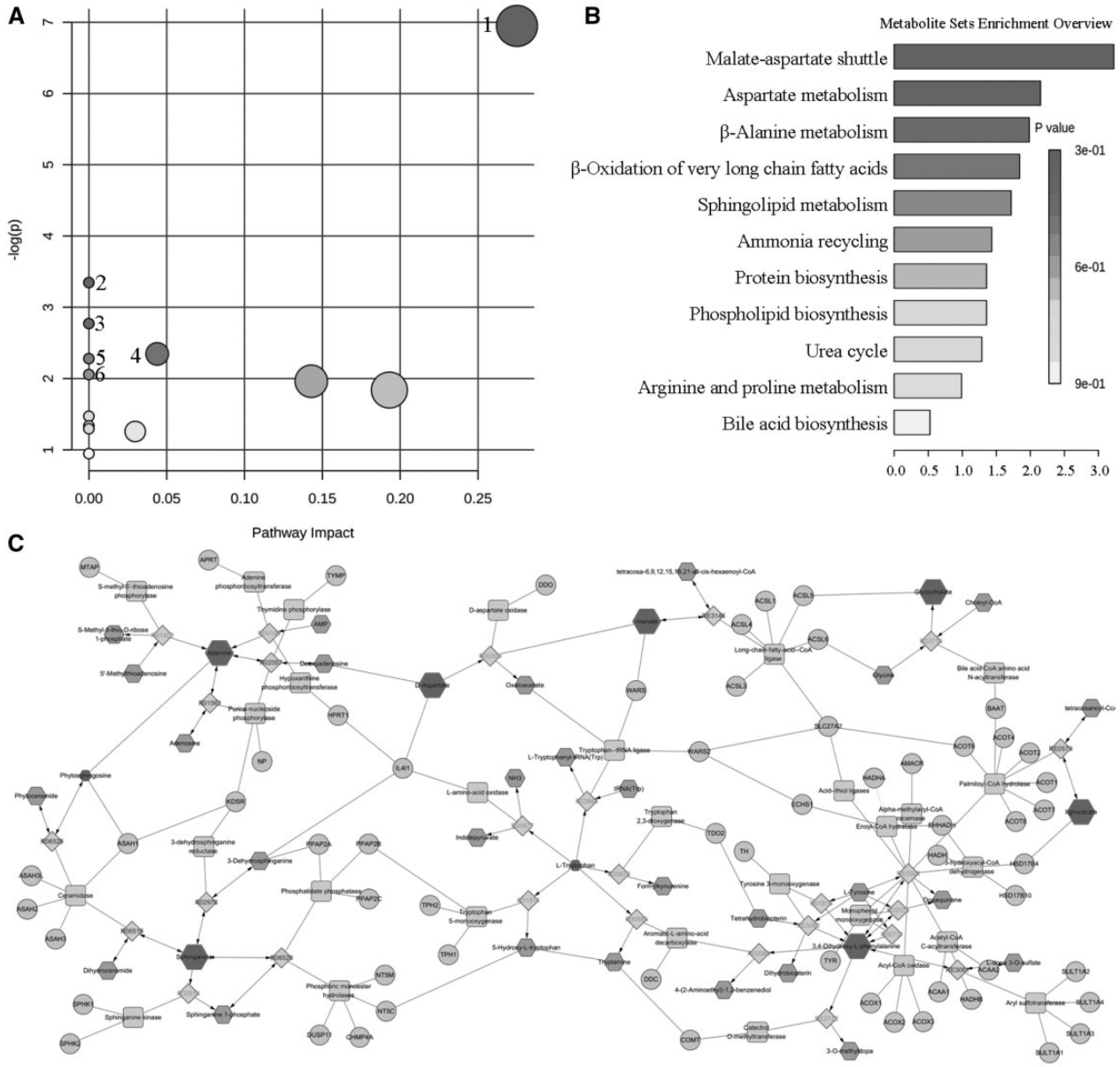

FIGURE 6: Metaboanalyst analysis of altered metabolites in plasma from CKD rats compared with control rats. (**A**) Metaboanalyst analysis using KEGG metabolic library. Both the altered metabolites in the pathway based on the hypergeometric test and the impact of the altered metabolites on the pathway function via alterations in critical junction points of the pathway were assessed. Results of each of the 81 rat pathways are simultaneously plotted to indicate the most significant pathways based on hypergeometric test P-value and impact. The top six pathways were found with low P-values or with high impact. (**B**) Metabolite enrichment pathway overview highlights malate-aspartate metabolism and long-chain fatty acids β-oxidation being remarkably enriched in the metabolomic profile of CKD rats compared with control rats. (**C**) Metabolic networks of amino acids, purine and lipids in CKD. The identified metabolites in current study were shown by red hexagons. Hexagons with green lines means that the significantly changes of the identified metabolite in CKD had statistical significance ($P < 0.05$). The size of hexagons showed the fold change of the differential metabolite in CKD relative to control. In addition, other graphs showed metabolites participating in the metabolic pathway but that had not been identified in the current study.

elongation and desaturation to eicosapentaenoic acid, and subsequently to docosahexaenoic acid, which are the substrates for generation of anti-inflammatory mediators. PUFA are highly vulnerable to ROS-mediated peroxidation, which makes them the target of endocytosis by macrophages. Unlike saturared fatty acids, plasma concentration of PUFA was significantly reduced in our CKD animals. Given the well-known association of CKD with oxidative stress the CKD-associated oxidative stress may have contributed to the depletion of the circulating PUFAs in these animals. By replacing arachidonic acid, long-chain n-3 PUFA found in fish and fish oils, can attenuate oxidative stress and inflammation by lowering production of inflammatory eicosanoids and, thereby, cytokines, adhesion molecules and ROS [38]. Therefore, deficiency of these PUFA may contribute to the CKD-associated systemic oxidative stress and inflammation. In fact, ω-3 supplementation in dialysis patients has been shown to lower triglyceride levels, raise dialysis access patency, and perhaps uremic pruritus and oxidative stress [39]. Moreover, ω-3 fatty

acids have been shown to limit the severity of formaldehyde-induced nephropathy in experimental animals and docosahexaenoic acid has been shown to enhance the antioxidant response in human fibroblasts by upregulating expression of gamma glutamyl-cysteinyl ligase and glutathione reductase [40, 41]. In addition, animal experiments have shown that PUFA increase superoxide dismutase and glutathione peroxidase enzyme activities, and decrease malondialdehyde level [41]. Therefore, the observed changes in the composition of the circulating fatty acids in CKD animals can, in part, contribute to the systemic inflammation, oxidative stress and progression of renal disease.

The CKD animals employed in the present study exhibited significant alterations in serum concentrations of amino acids. Earlier studies have found significant increase in serum phenylalanine and aspartic acid and significant decrease in tryptophan level in rats with adenine-induced CKD [42–44]. The reduction of tryptophan in this model has been attributed to increased energy and protein expenditure [4]. Aspartic acid concentration in CKD rats was significantly increased compared with the control group, which is in agreement with previously published data [45]. In fact, elevated serum aspartic acid correlates with the presence and severity of nephropathy in diabetic patients and as such represents a serum biomarker of diabetic nephropathy [46]. An earlier study revealed that serum aspartic acid level was significantly increased in end-stage renal disease patients before hemodialysis and after hemodialysis, and valine/glycine and tyrosine/phenylalanine ratios were significantly decreased in all patients on dialysis compared with controls [47].

CONCLUSIONS

UPLC-HDMS-based metabolomic and lipidomic analyses of serum from CKD rats with adenine-induced chronic interstitial nephropathy revealed profound alterations in serum concentrations of numerous metabolites including amino acids, fatty acid, phospholipids, glycerolipids and sphingolipids. This was associated with activation of NF-κB, up-regulation of pro-inflammatory, pro-oxidant and pro-fibrotic proteins, and down-regulation of Nrf2 activity and its down-stream antioxidant and cytoprotective proteins. Future studies are needed to explore the underlying mechanisms of the observed abnormalities and to determine the metabolomic and lipidomic impact of other forms of CKD in animals and humans.

SUPPLEMENTARY DATA

Supplementary data are available online at https://academic.oup.com/ndt.

ACKNOWLEDGEMENTS

This study was supported by the National Natural Science Foundation of China (Nos 81673578, 81603271), the Program for the New Century Excellent Talents in University of Ministry of Education of China (No NCET-13-0954) and the project As a Major New Drug to Create a Major National Science and Technology Special (No 2014ZX09304307-002).

CONFLICT OF INTEREST STATEMENT

None declared.

REFERENCES

1. Weiss RH, Kim K. Metabolomics in the study of kidney diseases. *Nat Rev Nephrol* 2011; 8: 22–33
2. Keller BJ, Martini S, Sedor JR *et al.* A systems view of genetics in chronic kidney disease. *Kidney Int* 2012; 81: 14–21
3. Smith MP, Banks RE, Wood SL *et al.* Application of proteomic analysis to the study of renal diseases. *Nat Rev Nephrol* 2009; 5: 701–712
4. Zhao YY. Metabolomics in chronic kidney disease. *Clin Chim Acta* 2013; 422: 59–69
5. Zhao YY, Lin RC. Metabolomics in nephrotoxicity. *Adv Clin Chem* 2014; 65: 69–89
6. Zhang ZH, Chen H, Vaziri ND *et al.* Metabolomic signatures of chronic kidney disease of diverse etiologies in the rats and humans. *J Proteome Res* 2016; 15: 3802–3812
7. Chen H, Cao G, Chen DQ *et al.* Metabolomics insights into activated redox signaling and lipid metabolism dysfunction in chronic kidney disease progression. *Redox Biol* 2016; 10: 168–178
8. Zhao YY Cheng XL Vaziri ND *et al.* UPLC based metabolomics applications for discovering biomarkers of diseases in clinical chemistry. *Clin Biochem* 2014; 47: 16–26
9. Zhao YY, Lei P, Chen DQ *et al.* Renal metabolic profiling of early renal injury and renoprotective effects of Poria cocos epidermis using UPLC Q-TOF/HSMS/MS^{E}. *J Pharm Biomed Anal* 2013; 81–82: 202–209
10. Zhao YY, Wu SP, Liu S *et al.* Ultra-performance liquid chromatography-mass spectrometry as a sensitive and powerful technology in lipidomic applications. *Chem Biol Interact* 2014; 220: 181–192
11. Vaziri, ND. Dyslipidemia of chronic renal failure: the nature, mechanisms and potential consequences. *Am J Physiol Renal Physiol* 2006; 290: 262–272
12. Vaziri ND. Molecular mechanisms of lipid disorders in nephrotic syndrome. *Kidney Int* 2003; 63: 1964–1976
13. Zhang ZH, Wei F, Vaziri ND *et al.* Metabolomics insights into chronic kidney disease and modulatory effect of rhubarb against tubulointerstitial fibrosis. *Sci Rep* 2015; 5: 14472
14. Zhang ZH, Vaziri ND, Wei F *et al.* An integrated lipidomics and metabolomics reveal nephroprotective effect and biochemical mechanism of Rheum officinale in chronic renal failure. *Sci Rep* 2016; 6: 22151
15. Zhao YY, Liu J, Cheng XL *et al.* Urinary metabonomics study on biochemical changes in an experimental model of chronic renal failure by adenine based on UPLC Q-TOF/MS. *Clin Chim Acta* 2012; 413: 642–649
16. Vaziri ND. Lipotoxicity and impaired HDL-mediated reverse cholesterol/lipid transport in chronic kidney disease. *J Ren Nutr* 2010; 20: S35–S43
17. Vaziri ND, Norris K. Lipid disorders and their relevance to outcomes in chronic kidney disease. *Blood Purif* 2011; 31: 189–196
18. Vaziri ND. Role of dyslipidemia in impairment of energy metabolism, oxidative stress, inflammation and cardiovascular disease in chronic kidney disease. *Clin Exp Nephrol* 2014; 18: 265–268
19. Wyngaarden JB, Dunn JT. 8-Hydroxyadenine as the metabolic intermediate in the oxidation of adenine to 2,8-dihydroxyadenine by xanthine oxidase. *Arch Biochem Biophys* 1957; 70: 150–156
20. Zhao YY, Chen H, Tian T *et al.* A pharmaco-metabonomic study on chronic kidney disease and therapeutic effect of ergone by UPLC-QTOFHDMS. *PLoS One* 2014; 9: e115467
21. Zhao YY, Shen X, Cheng XL, *et al.* Urinary metabonomics study on the protective effects of ergosta-4,6,8(14),22-tetraen-3-one on chronic renal failure in rats using UPLC Q-TOF/MS and a novel MS^{E} data collection technique. *Process Biochem* 2012; 47: 1980–1987

22. Zhao YY, Cheng XL, Wei F *et al.* Intrarenal metabolomic investigation of chronic kidney disease and its TGF-β1 mechanism in induced-adenine rats using UPLC Q-TOF/HS-MS/MS^{E}. *J Proteome Res* 2013; 12: 692–703
23. Zhao YY, Wang HL, Cheng XL *et al.* Metabolomics analysis reveals the association between lipid abnormalities and oxidative stress, inflammation, fibrosis, and Nrf2 dysfunction in aristolochic acid-induced nephropathy. *Sci Rep* 2015; 5: 12936
24. Xia J, Wishart DS. MSEA: a web-based tool to identify biologically meaningful patterns in quantitative metabolomic data. *Nucleic Acids Res* 2010; 38: W71–W77
25. Karnovsky A, Weymouth T, Hull T *et al.* Metscape 2 bioinformatics tool for the analysis and visualization of metabolomics and gene expression data. *Bioinformatics* 2012; 28: 373–380
26. Vaziri ND. Oxidative stress in uremia: nature, mechanisms, and potential consequences. *Semin Nephrol* 2004; 24: 469–473
27. Sies H. Oxidative stress: oxidants and antioxidants. *Exp Physiol* 1997; 82: 291–295
28. Kim HJ, Vaziri ND. Contribution of impaired Nrf2-Keap1 pathway to oxidative stress and inflammation in chronic renal failure. *Am J Physiol Renal Physiol* 2010; 298: F662–F671
29. Ruiz S, Pergola PE, Zager RA *et al.* Targeting the transcription factor Nrf2 to ameliorate oxidative stress and inflammation in chronic kidney disease. *Kidney Int* 2013; 83: 1029–1041
30. Locatelli F, Canaud B, Eckardt KU *et al.* Oxidative stress in end-stage renal disease: an emerging threat to patient outcome. *Nephrol Dial Transplant* 2003; 18: 1272–1280
31. Suresh DR, Delphine S, Agarwal R. Biochemical markers of oxidative stress in predialytic chronic renal failure patients. *Hong Kong J Nephrol* 2008; 10: 69–73
32. Wang L, Hu C, Liu S *et al.* Plasma lipidomics investigation of hemodialysis effects by using liquid chromatography-mass spectrometry. *J Proteome Res* 2016; 15: 1986–1994
33. Friedman AN, Yu Z, Denski C *et al.* Fatty acids and other risk factors for sudden cardiac death in patients starting hemodialysis. *Am J Nephrol* 2013; 38: 12–18
34. Kang HM, Ahn SH, Choi P *et al.* Defective fatty acid oxidation in renal tubular epithelial cells has a key role in kidney fibrosis development. *Nat Med* 2015; 21: 37–46
35. Susztak K, Ciccone E, McCue P *et al.* Multiple metabolic hits converge on CD36 as novel mediator of tubular epithelial apoptosis in diabetic nephropathy. *PLoS Med* 2005; 2: e45
36. Schug TT, Li X. Sirtuin 1 in lipid metabolism and obesity. *Ann Med* 2011; 43: 198–211
37. Dugan LL, You YH, Ali SS *et al.* AMPK dysregulation promotes diabetes-related reduction of superoxide and mitochondrial function. *J Clin Invest* 2013; 123: 4888–4899
38. Calder PC. n-3 polyunsaturated fatty acids, inflammation, and inflammatory diseases. *Am J Clin Nutr* 2006; 833: 1505–1519
39. Friedman A, Moe S. Review of the effects of omega-3 supplementation in dialysis patients. *Clin J Am Soc Nephrol* 2006; 1: 182–192
40. Zararsiz I, Sonmez MF, Yilmaz HR *et al.* Effects of omega-3 essential fatty acids against formaldehyde-induced nephropathy in rats. *Toxicol Ind Health* 2006; 22: 223–229
41. Arab K, Rossary A, Flourié F *et al.* Docosahexaenoic acid enhances the antioxidant response of human fibroblasts by upregulating gammaglutamylcysteinyl ligase and glutathione reductase. *Br J Nutr* 2006; 95: 18–22
42. Zhao YY, Cheng XL, Wei F *et al.* Serum metabonomics study of adenine-induced chronic renal failure in rats by ultra performance liquid chromatography coupled with quadrupole time-of-flight mass spectrometry. *Biomarkers* 2012; 17: 48–55
43. Zhao YY, Cheng XL, Cui JH *et al.* Effect of ergosta-4,6,8(14),22-tetraen-3-one (ergone) on adenine-induced chronic renal failure rat: a serum metabonomics study based on ultra performance liquid chromatography/high-sensitivity mass spectrometry coupled with MassLynx i-FIT algorithm. *Clin Chim Acta* 2012; 413: 1438–1445
44. Zhao YY, Feng YL, Bai X *et al.* Ultra performance liquid chromatography-based metabonomic study of therapeutic effect of the surface layer of Poria cocos on adenine-induced chronic kidney disease provides new insight into anti-fibrosis mechanism. *PLoS One* 2013; 8: e59617
45. Yokozawa T, Zheng PD, Oura H *et al.* Animal model of adenine-induced chronic renal failure in rats. *Nephron* 1986; 44: 230–234
46. Hirayama A, Nakashima E, Sugimoto M *et al.* Metabolic profiling reveals new serum biomarkers for differentiating diabetic nephropathy. *Anal Bioanal Chem* 2012; 404: 3101–3109
47. Chuang CK, Lin SP, Chen HH *et al.* Plasma free amino acids and their metabolites in Taiwanese patients on hemodialysis and continuous ambulatory peritoneal dialysis. *Clin Chim Acta* 2006; 364: 209–216

Received for publication: 5.9.2016; Accepted in revised form: 12.10.2016